

Shape Optimisation and Performance Analysis of Flapping Wings

M. Ghommem, N. Collier, A.H. Niemi and V.M. Calo
King Abdullah University of Science and Technology (KAUST)
Thuwal, Kingdom of Saudi Arabia

Abstract

In this paper, we consider the shape optimization of flapping wings in forward flight. This analysis is performed by combining a gradient-based optimiser with the unsteady vortex lattice method. The objective is to identify a set of optimised shapes that maximise the propulsive efficiency under lift, thrust, and area constraints. The geometry of the wings is modelled using B-splines. The flow simulations using the optimal wing shapes indicate that changes in the shape have significant effects on averaged quantities. The optimal shape configuration substantially increases the time averaged thrust while, at the same time, it acquires a larger input of aerodynamic power. Increasing the number of variables (*i.e.*, providing the wing shape with a greater degree of spatial freedom) enables increasingly superior designs. This study should provide better guidance for shape design of engineered flying systems.

Keywords: unsteady vortex lattice method, flapping wings, B-splines, shape optimization.

1 Introduction

Micro-air vehicles (MAVs) are small flying aeroelastic systems that are expected to operate in urban environments and confined spaces (*i.e.*, inside buildings, caves, tunnels). A variety of missions can be assigned to these systems such as inspection of harsh environments inaccessible to other types of vehicles. To successfully achieve the aforementioned missions, these systems must be designed to satisfy stringent performance requirements, such as high maneuverability at low speeds, hovering capabilities, high lift to sustain flight, and structural strength to survive gust loads. These requirements can be achieved mainly through two propulsion mechanisms: rotating helicopter blades or flapping wings [1]. Through observing the efficiency of insects

and birds, it has been concluded that flapping wings offer greater efficiency, especially at small scales [2–5]. Studying these flying animals as a step toward designing flapping-wing vehicles has been the topic of many investigations [6–13].

Although it is well known that natural flyers exploit a variety of mechanisms and aerodynamic aspects to control and manoeuvre their flights, experimental observations do not enable a good understanding of the physical aspects and dynamics of flapping flight. As such, there is a need to model the unsteady aerodynamic aspects of flapping-wing vehicles. Computational modeling and simulation are necessary to evaluate the performance requirements associated with flapping flight and identify the relative impact of design parameters (e.g., flapping parameters, shape characteristics). Several computational modeling strategies that are based on variable fidelity physics have been reported in the literature [14–21]. Willis et al. [22] developed a multifidelity computational framework that involves a combination of potential flow models and Navier-Stokes solver. They showed how the use of models with different levels of geometric and physical modeling fidelity can be well exploited to ease the design process of flapping wing systems. Certainly, the higher-fidelity Navier-Stokes simulations incorporate a more complete physical model of the flapping flight problem, however, the extensive computational resources and time associated with the use of these tools limit the ability to perform optimization and sensitivity analyses in the early stages of MAV design. Thus, to alleviate this burden and enable rapid and reasonably accurate exploration of a large design space, it is fairly common to rely upon a moderate level of modeling fidelity to traverse the design space in an economical manner [23, 24]. As such, several research efforts have considered the use of the unsteady vortex lattice method (UVLM) for the design of avian-like flapping wing in forward flight [14, 25–28].

In this work, we consider shape optimization of flapping wings in forward flight. This is performed by combining a local gradient-based optimizer with UVLM. Although UVLM applies only to incompressible, inviscid flows where the separation lines are known a priori, Persson et al. [16] showed through a detailed comparison between UVLM and higher-fidelity computational fluid dynamics methods for flapping flight that the UVLM schemes produce accurate results for attached flow cases and even remain trend-relevant in the presence of flow separation. As such, in [16] they recommended the use of an aerodynamic model based on UVLM to perform preliminary standard design studies of flapping wing vehicles (especially in desirable cruise configurations where there is no flow separation and substantial wing-wake interactions that would degrade the performance of the vehicle). Furthermore, the associated simulation time is on the order of few minutes on a desktop. Our objective in this paper is to identify a set of optimized shapes that maximize the propulsive efficiency under lift, thrust, and area constraints. The geometry of the wings is modeled using B-splines. This basis can be used to smoothly discretize wing shapes with few degrees of freedom, referred to as control points. The locations of the control points constitute the design variables. Results suggest that changing the shape yields significant improvement in the flapping wings performance. This study is our first stop towards constructing a framework that will facilitate the design of engineered flying systems.

2 Aerodynamic Modeling of Flapping Wings

We use the three-dimensional version of the unsteady vortex lattice method (3-D UVLM) to simulate the aerodynamic response of flapping wings in forward flight. This aerodynamic tool is capable of simulating incompressible and inviscid flow past moving thin wings and capturing the unsteady effects of the wake, but not the viscous effects, flow separation at the leading-edge, and extreme situations with strong wing-wake interactions. Unlike standard computational fluid dynamics schemes, this method requires meshing of the wing planform only and not of the whole flow domain. Thus, UVLM reduces the demand for computational resources. These features make it competitive to perform optimization studies that require many simulations.

Features of the used UVLM solver include the following

- The shape of the wing is generated based on B-spline representation.
- The wing surface is discretized into a lattice of vortex rings. Each vortex ring consists of four short straight vortex segments, with a collocation point placed at its center.
- For rigid wings, the grid points position is specified by applying a sequence of rotations (pitching and flapping).
- The no-penetration condition is imposed at the collocation points (i.e., the normal component of the velocity at each collocation point due to wing-wing interactions, wake-wing interactions, free-stream velocities, and wing rotations should vanish). Using the Biot-Savart law to compute velocities in terms vorticity circulations Γ yields a linear system of equations

$$A^{wi-wi} \cdot \Gamma_{wi} = -A^{wa-wi} \cdot \Gamma_{wa} + V_n \quad (1)$$

where A^{wi-wi} and A^{wa-wi} are wing-wing and wake-wing influence matrices, respectively, and V_n is a vector collecting the normal component of the velocity at each collocation point due to the wing motion [14].

- The vorticity is introduced into the wake by shedding vortex segments from the trailing edge. These vortices are moved with the fluid particle velocity and their individual circulation remains constant (i.e., $\Gamma_{wa}^{t+\Delta t} = \Gamma_{te}^t$).
- The pressure is evaluated at each collocation point based on the unsteady Bernoulli equation and then integrated over the wing surface to compute the aerodynamic forces and power.

Further details of the derivation, implementation, and verification of this method and aerodynamic loads computation are provided in [14, 27, 29, 30].

3 Modeling of Wing Shape: B-splines Representation

3.1 B-spline curves and surfaces

B-splines are piecewise polynomials based on the Bernstein basis. The basis functions of degree p , denoted by $N_{i,p}(\xi)$, associated to a non-decreasing set of coordinates called the knot vector $\mathcal{X} = \{\xi_1, \xi_2, \dots, \xi_{n+p+1}\}$ are defined recursively as

$$N_{i,0}(\xi) = \begin{cases} 1, & \xi_i \leq \xi < \xi_{i+1} \\ 0, & \text{otherwise} \end{cases}$$

$$N_{i,p}(\xi) = \frac{\xi - \xi_i}{\xi_{i+p} - \xi_i} N_{i,p-1}(\xi) + \frac{\xi_{i+p+1} - \xi}{\xi_{i+p+1} - \xi_{i+1}} N_{i+1,p-1}(\xi), \quad p > 0$$

for $i = 1, \dots, n$ and $p \geq 1$. Knot multiplicities reduce the continuity of the basis at the location of the multiplicity. If a multiplicity of k knots is used, the continuity on the basis is C^{p-k} at that knot. Consequently, the basis becomes interpolatory at knots with multiplicity p whereas knot multiplicity of $p + 1$ makes the basis discontinuous and is used at the end points to make the knot vector open.

The B-spline curve of degree p with control points $\mathbf{P}_1, \dots, \mathbf{P}_n$ is defined on the interval $[a, b] = [\xi_{p+1}, \xi_{n+1}]$ as the linear combination of the control points and basis functions

$$\mathbf{C}(\xi) = \sum_{i=1}^n N_{i,p}(\xi) \mathbf{P}_i$$

The piecewise linear interpolation of the control points is called the control polygon. A feature of B-spline curves is that the curve defined by the basis and control points will lie inside of the convex hull of the control polygon. This makes the control polygon useful for approximating the rough character of a curve.

A B-spline surface is defined using tensor products of B-spline basis functions written in two parametric coordinates ξ, η . If $N_{i,p}$ and $M_{j,q}$ denote basis functions of degree p and q associated to the knot vectors $\mathcal{X} = \{\xi_1, \xi_2, \dots, \xi_{n+p+1}\}$ and $\mathcal{Y} = \{\eta_1, \eta_2, \dots, \eta_{m+q+1}\}$ and $\mathbf{P}_{ij}, i = 1, \dots, n, j = 1, \dots, m$ is a net of control points in three-dimensional space, the B-spline surface is defined as

$$\mathbf{S}(\xi, \eta) = \sum_{i=1}^n \sum_{j=1}^m N_{i,p}(\xi) M_{j,q}(\eta) \mathbf{P}_{ij}$$

B-splines have long been used in the computer aided design community to model curves and surfaces. The reader is referred to [31–34] for more details on B-splines.

3.2 Wing shape parametrization

In Figure 1, we plot the wing geometry model based on B-splines representation. To enable changes in the wing shape, the control points that define the curvatures of the

leading and trailing edges (blue spheres) are allowed to move along y -direction and those that specify the wing tip (green spheres) are allowed to move in both x and y directions. The interior points are distributed so that the camber line is preserved at each cross section once the locations of the control points at the edges are specified. The control point represented by black sphere is kept fixed.

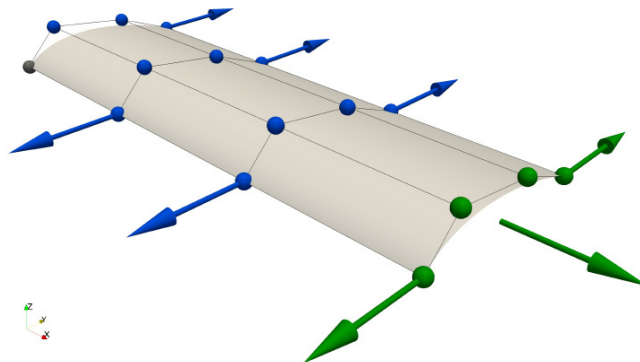


Figure 1: Wing geometry model based on B-spline representation. Spheres are used to represent the control points and arrows denote their perturbation directions.

4 Shape Optimization

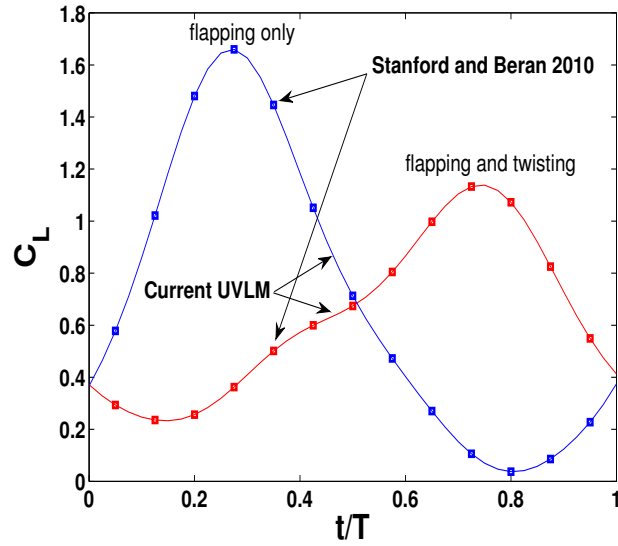
In this section, we consider cambered rectangular wings with an aspect ratio of six (baseline case). The cambered wing has a NACA 83XX cross-sectional profile as studied previously by Stanford and Beran [14] and Ghommem et al. [27]. The symmetric flapping motion (about the wing root) is prescribed as given by:

$$\phi(t) = A_\phi \cos(\omega t), \quad (2)$$

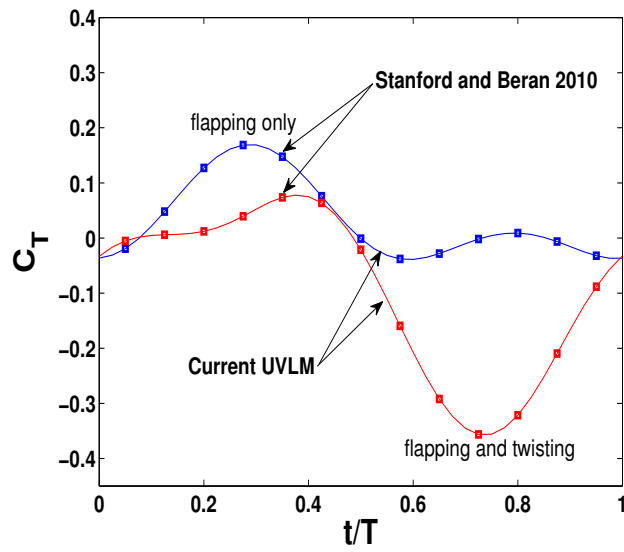
where ϕ is the flapping angle and the flapping amplitude A_ϕ is set equal to 45° . Furthermore, the wing root is placed at a fixed angle of attack (pitch) of 5° . A reduced frequency $\kappa = 0.1$ is used. The reduced frequency is defined as

$$\kappa = \frac{\omega}{U_\infty} \cdot \frac{c}{2},$$

where ω is the flapping frequency, c is the chord length, and U_∞ is the freestream velocity. The transient variations of the lift and thrust over one flapping cycle predicted by the current UVLM and those obtained by Stanford and Beran [14] are shown in Figure 2. A good agreement can be clearly observed. The untwisted flapping wing case constitutes the baseline case of the optimization studies conducted next. We note that for the twisted wing case, the twisting is sinusoidal (out-of-phase with respect to the flapping motion) and varies linearly along the span so that the maximum twist is obtained at the tip with an amplitude equal to 45° .



(a) Lift coefficient



(b) Thrust coefficient

Figure 2: Lift and thrust computed from UVLM for one flapping cycle, with and without wing twisting: comparison with results obtained by Stanford and Beran [14]. Six elements are used along the chordwise direction and ten are used along the spanwise direction (for half wing).

4.1 Problem formulation

Flapping wings must be designed to satisfy some performance requirements such as capability to generate required aerodynamic forces to hold the body, sustain forward flights, and survive gust loads. In particular, wing shapes selection constitutes an important component in the design process. As such, we adopt the B-splines representation to model the wing shape and combine UVLM with a gradient-based optimization algorithm to conduct series of optimization studies. This would help in identifying a suitable set of wing shapes that enable efficient flights. The optimization problem is formulated as follows:

$$\begin{aligned} & \text{maximize } \eta \\ & \text{subject to: } \begin{cases} \mathbf{x}_{min} \leq \mathbf{x} \leq \mathbf{x}_{max}, \\ \overline{L^*} \geq \overline{L^*}_{bl}, \\ \overline{T^*} \geq \overline{T^*}_{bl}, \\ \max |\theta_i - \frac{\pi}{2}| \leq \theta_{cr}, \\ A \leq A_{bl}, \end{cases} \end{aligned} \quad (3)$$

where \mathbf{x} is the vector of design parameters describing the perturbations introduced to the locations of the control points,

$$L^* = L/(0.5\rho U_\infty^2), \quad T^* = T/(0.5\rho U_\infty^2), \quad \text{and} \quad P^* = P/(0.5\rho U_\infty^3)$$

are the normalized lift, thrust, and aerodynamic power, respectively, A is the wing's area, and the overline denotes a time-averaged quantity over a flapping cycle. The wing geometry is constrained by bounding the feasible perturbations of the locations of the control points ($\pm 0.5 \cdot c$). Here, the main objective is to maximize the cycle-averaged propulsive efficiency of the wing under lift and thrust constraints. The propulsive efficiency is defined as the ratio of the propulsive power over the aerodynamic power [14, 27]. The area of the wing is also restricted to be smaller or equal to a baseline value (i.e., the area of a cambered rectangular wing with an aspect ratio of six). Besides, we add a constraint to monitor the angles θ_i of each element to avoid large distortions and curvatures of the mesh grid that would degrade the predictive capability of the aerodynamic model and also may give rise to undesirable (in cruise flapping flight) unsteady flow effects (e.g., flow separation, substantial wing-wake interactions). θ_{cr} is set equal to 15° . The optimization problem is solved with the globally convergent method of moving asymptotes (GCMMA) [35, 36], where the algorithm is supplied with numerically-computed gradients based on the first-order backward Euler scheme for both the objective function and the constraints. Several optimization runs are conducted where we vary the number of design variables and the polynomial order of the basis functions employed in the B-splines representation. These simulations elucidate the effect of the design parameters on the numerical results.

4.2 Results and discussion

We consider the case where the B-splines representation is based on a single element. Thus, the number of control points increases with the order of polynomials. Table 1 provides a summary of the efficiency η , lift L^* , thrust T^* , aerodynamic power P^* , and area ratio A/A_{bl} obtained for the optimal configurations for different polynomial orders. The optimal results show that changing the wing shape would allow to achieve higher lift and propulsive efficiency but also more power is needed to be introduced to the flying system. In Figure 3, we show the progress that the gradient-based optimizer GCMMA makes in maximizing the propulsive efficiency when considering different polynomials for the B-splines basis functions. The GCMMA optimization tool is observed to identify a maximum within few iterations (~ 40 iterations). The optimization algorithm GCMMA was supplied with different starting points and led to the same optimal points. This robustness indicates that the objective function (propulsive efficiency) associated with the flapping flight is approximately quasiconcave so that GCMMA is insensitive to the initial guess. This observation is not valid for arbitrary design spaces associated with flapping problem [30]. As expected, increasing the polynomial order (i.e., specifying more control points) yields optimal shapes that enable flapping flights with higher efficiencies. The use of linear polynomials which yields a tapered wing ameliorates the flapping performance. The area convergence histories, shown in Figure 3(b), indicate that the area constraint is active for all cases. Figure 4 provides the set of optimal shapes obtained for different polynomials. A noticeable change in the wing shape can be observed and this is accompanied with an improvement in the propulsive efficiency.

Wing shape		N_{DV}	η	L^*	T^*	P^*	A/A_{bl}
Baseline shape		0	0.191	4.171	0.196	1.028	1
Optimal shapes	Linear	6	0.311	5.021	0.413	1.327	1
	Quadratic	8	0.347	4.882	0.502	1.446	1
	Cubic	10	0.353	5.061	0.472	1.336	1
	Quartic	12	0.360	5.012	0.501	1.393	1

Table 1: Baseline vs. optimal results.

The lift, thrust, and aerodynamic power, that develop over the flapping wing at $\kappa = 0.1$ for both the baseline and optimal cases, plotted as function of the flapping angle ϕ are given in Figure 5. As expected, the bulk of the useful aerodynamic forces (positive lift and thrust) is generated during the downstroke. In particular, peaks of thrust and lift are reached near the middle of the downstroke phase. Positive lift is produced during both strokes, as the angle of attack induced by the flapping motion is smaller than the fixed pitch angle (5°) at the wing root, and thus the lift remains positive through almost the entire cycle. The optimal shape does not alter the phases of the aerodynamic quantities, since the effective angle of attack does not vary significantly over the flapping cycle. Nevertheless, it is able to increase the time-averaged lift,

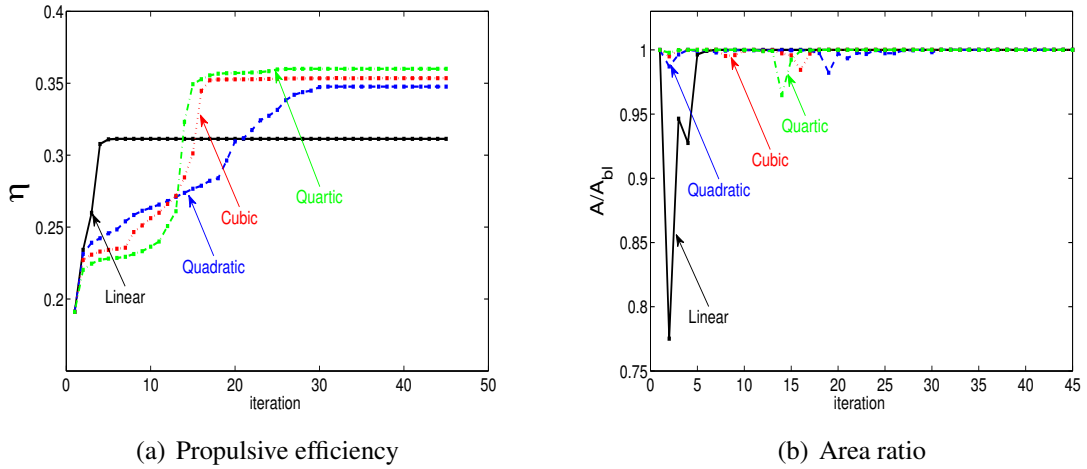


Figure 3: The efficiency and normalized area values at the best point found versus the number of iterations from GCMMA using different polynomials.

thrust, and power (as seen in Table 1), as well as their peaks as shown in Figure 5.

The vorticity in the wake was generated on and shed from the wing at an earlier time. As such, the wake is usually referred as the "historian" of the flow. Thus, examining the wake pattern and vorticity distribution can be helpful to determine the reasons why the obtained optimized shapes produce efficient flapping flights. The vorticity circulation strength of the wakes obtained for the baseline and optimal wing shapes is given in Figure 6. Clearly, the overall strength of the wake has increased in comparison with the baseline case, as the average aerodynamic power has increased as shown in Table 1. In particular, stronger pockets of high circulation are observed in the wake aft of the optimal shape at the middle of the down and upstrokes (i.e., $\phi \approx 0^\circ$). Furthermore, we remark that the vortex tip swirl is more pronounced for the baseline shape. So, the optimal shape managed to reduce the tip vortex effect and then produces higher thrust.

5 Conclusion

In this paper, we study the shape optimisation of flapping wings in forward flight. This was performed by combining the unsteady vortex lattice method with a gradient-based optimizer while using B-splines representation to model the wing geometry. The wing shape plays an important role in the performance of flapping flight, in particular, the curvatures at the leading and trailing edges. The optimization pushes the design to a shape configuration with substantial increase in the time-averaged thrust, while the average aerodynamic power is increased, resulting in a significant increase in the propulsive efficiency.

This work was concerned solely with the assessment of the aerodynamic perfor-

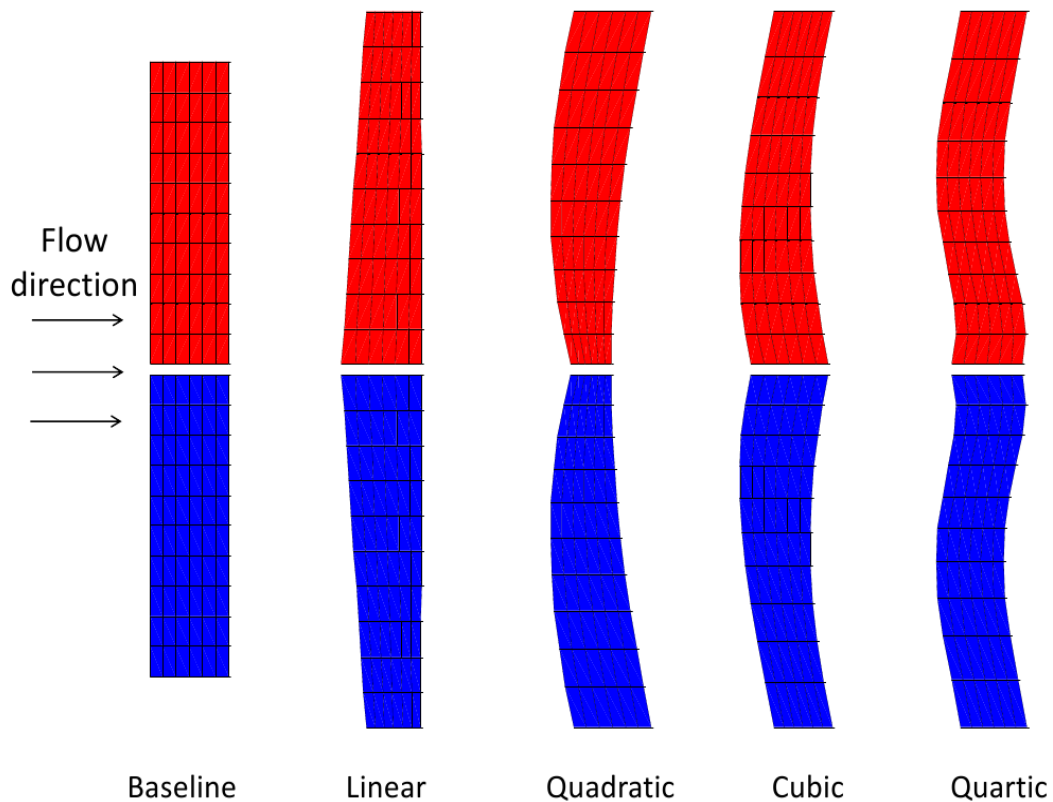


Figure 4: Optimal wing shapes.

mance of rigid flapping wings when considering different shapes. Implementing a full aeroelastic framework that couples a nonlinear shell model and UVLM to test the obtained optimal shapes and check their superiority over the baseline configuration is the topic of our current research effort. Preliminary simulation results to validate the shell formulation are presented in [37].

Acknowledgment

The authors thank Prof. Svanberg who kindly provided the optimization package GCMMA.

References

- [1] L. Petricca, P. Ohlckers, C. Grinde, “Micro- and Nano-Air Vehicles: State of the Art”, *International Journal of Aerospace Engineering*, 2011, Article ID 214549, 17 pages, doi:10.1155/2011/214549.

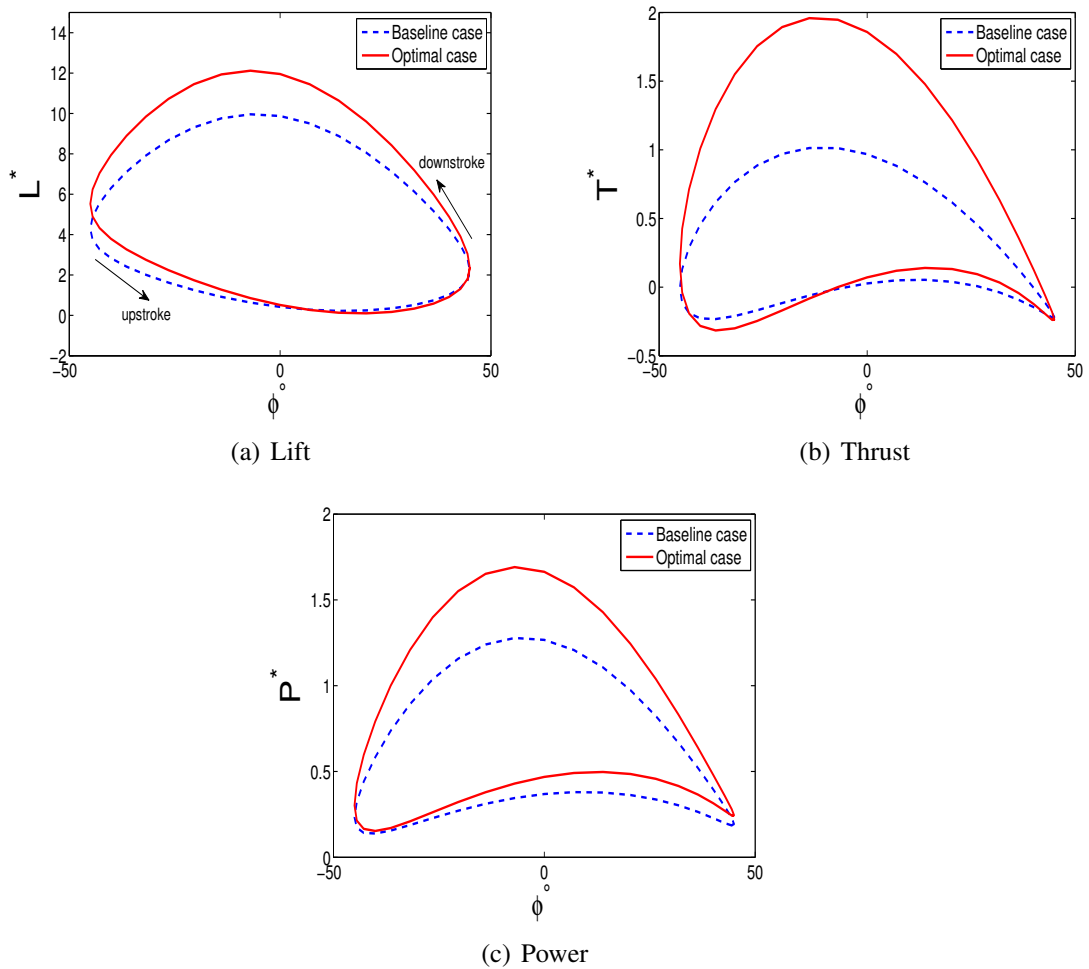


Figure 5: Lift, thrust, and power plotted versus the flapping angle ϕ for the baseline (rectangular) and optimal shapes (cubic polynomial).

- [12] B.W. Tobalske, D.R. Warrick, C.J. Clark, D.R. Powers, T.L. Hedrick, G.A. Hyder, A.A. Biewener, “Three-Dimensional Kinematics of Hummingbird Flight”, *Journal of Experimental Biology*, 210: 2368–2382, 2007.
- [13] X. Tian, J. Iriarte-Diaz, K. Middleton, R. Galvao, E. Israeli, A. Roemer, A. Sullivan, A. Song, S. Swartz, K. Breuer, “Direct Measurements of the Kinematics and Dynamics of Bat Flight”, *Bioinspiration and Biomimetics*, pages 10–18, 2006.
- [14] B.K. Stanford, P.S. Beran, “Analytical Sensitivity Analysis of an Unsteady Vortex-Lattice Method for Flapping-Wing Optimization”, *Journal of Aircraft*, 47: 647–662, 2010.
- [15] S.E. Bansmer, R. Radespiel, “Validation of Unsteady Reynolds-Averaged Navier-Stokes Simulations on Three-Dimensional Flapping Wings”, *AIAA Journal*, 50: 190–202, 2012.
- [16] P. Persson, D. Willis, J. Peraire, “Numerical Simulation of Flapping Wings Using a Panel Method and High-Order Navier-Stokes Solver”, *International Journal for Numerical Methods in Engineering*, 89: 1296–1316, 2012.
- [17] M. Ghommem, M. Hajj, L. Watson, D. Mook, R. Snyder, P. Beran, “Deterministic global optimization of flapping wing motions for micro air vehicles”, in *Proceedings of the 13th AIAA/ISSMO Multidisciplinary Analysis Optimization Conference*. AIAA Paper No. 2006-1852, 2010.
- [18] G.J. Berman, Z.J. Wang, “Energy-Minimizing Kinematics in Hovering Insect Flight”, *Journal of Fluid Mechanics*, 582: 153–168, 2007.
- [19] W. Yuan, R. Lee, E. Hoogkamp, M. Khalid, “Numerical and Experimental Simulations of Flapping Wings”, *International Journal of Micro Air Vehicles*, 2: 181–209, 2010.
- [20] H. Liu, “Integrated Modeling of Insect Flight: From Morphology, Kinematics to Aerodynamics”, *Journal of Computational Physics*, 228: 439–459, 2009.
- [21] S.P. Sane, M.H. Dickinson, “The Aerodynamics Effects of Wing Rotation and a Revised Quasi-steady Model of Flapping Flight”, *Journal of Experimental Biology*, 205: 1087–1096, 2002.
- [22] D.J. Willis, P. Person, E.R. Israeli, J. Peraire, S.M. Swartz, K.S. Breuer, “Multifidelity Approaches for the Computational Analysis and Design of Effective Flapping Wing Vehicles”, in *Proceedings of the 47th AIAA Aerospace Science Meeting and Exhibit*. AIAA Paper No. 2008-518, 2008.
- [23] B.K. Stanford, P.S. Beran, “Formulation of Analytical Design Derivatives for Nonlinear Unsteady Aeroelasticity”, *AIAA Journal*, 49: 598–610, 2011.
- [24] B. Stanford, P. Beran, M. Kobayashi, “Aeroelastic Optimization of Flapping Wing Venation: A Cellular Division Approach”, *AIAA Journal*, 50: 938–951, 2012.
- [25] M.S. Vest, J. Katz, “Unsteady Aerodynamic Model of Flapping Wings”, *AIAA Journal*, 34: 1435–1440, 1996.
- [26] T.E. Fritz, L.N. Long, “Object-Oriented Unsteady Vortex Lattice Method for Flapping Flight”, *Journal of Aircraft*, 41: 1275–1290, 2004.
- [27] M. Ghommem, M.R. Hajj, D.T. Mook, B.K. Stanford, P.S. Beran, L.T. Watson,

- “Global optimization of Actively-Morphing Flapping Wings,” *Journal of Fluids and Structures*, 2012, Under review.
- [28] M.J.C. Smith, P.J. Wilkin, M.H. Williams, “The Advantages of an Unsteady Panel Method in Modelling the Aerodynamic Forces on Rigid Flapping Wings”, *Journal of Experimental Biology*, 199: 1073–1083, 1996.
- [29] J. Katz, A. Plotkin, *Low-Speed Aerodynamics*, Cambridge University Press, MA, 2001.
- [30] M. Ghommem, *Modeling and Analysis for Optimization of Unsteady Aeroelastic Systems*, PhD thesis, Virginia Polytechnic Institute and State University, Blacksburg, VA, 2011.
- [31] D.F. Rogers, *An Introduction to NURBS With Historical Perspective*, Academic Press, San Diego, CA, 2001.
- [32] L. Piegl, W. Tiller, *The NURBS Book (Monographs in Visual Communication)*, 2nd ed., Springer-Verlag, New York, 1997.
- [33] G. Farin, *NURBS Curves and Surfaces: From Projective Geometry to Practical Use*, A. K. Peters, Ltd., Natick, MA, 1995.
- [34] E. Cohen, R. Riesenfeld, G. Elber, *Geometric Modeling with Splines. An Introduction*, A K Peters Ltd., Wellesley, Massachusetts, 2001.
- [35] K. Svanberg, “The Method of Moving Asymptotes– a New Method for Structural Optimization”, *International Journal for Numerical Methods in Engineering*, 24: 359–373, 1987.
- [36] K. Svanberg, “A Class of Globally Convergent Optimization Methods Based on Conservative Convex Separable Approximations”, *SIAM Journal on Optimization*, 12: 555–573, 2002.
- [37] A.H. Niemi, N.O. Collier, L. Dalcin, M. Ghommem, V.M. Calo, “Isogeometric Shell Formulation Based on Classical Shell Model”, in *The Eighth International Conference on Engineering Computational Technology*, 2012.